Curve Tracking for Rapid Imaging in AFM

Sean B. Andersson, *Member, IEEE*

***Abstract*—A high-level feedback control approach for rapid imaging in atomic force microscopy is presented. The algorithms are designed for samples which are string-like, such as biopolymers, and for boundaries. Rather than the simple raster-scan pattern, data from the microscope are used in real-time to steer the tip along the sample, drastically reducing the area to be imaged. An order-of-magnitude reduction in the time to acquire an image is possible. The technique is illustrated through simulations and through physical experiments.**

***Index Terms*—Atomic force microscopy, biomedical microscopy.**

I. Introduction

ATOMIC FORCE microscopes image samples by measuring the interaction force between a very sharp tip mounted at the end of a soft cantilever and the surface of the sample. As with all scanning probe microscopies, the measurement in atomic force microscopy (AFM) is a local one. As a result an image is built pixel-by-pixel by raster-scanning the tip with respect to the sample. Typical imaging times are on the order of minutes, depending on the size, resolution, and quality desired of the image. In this paper we present a high-level control approach to replace the raster-scan pattern. For string-like structures such as biopolymers (including DNA, actin, and microtubules), carbon nanotubes, and boundaries (including cell edges and crystal boundaries), our approach greatly decreases the amount of area to be imaged and can result in an order-of-magnitude reduction in the image acquisition time.

Due to its subnanometer resolution and ability to image a wide variety of samples, AFM has been remarkably effective at exploring structure in systems with nanometer-scale features. (See, for example, the survey papers [1]–[5].) There is growing interest in using the technology to explore the dynamics in systems at this scale [6]–[8]. The typical approach is time-lapse imaging (also known as time-resolved AFM) wherein a sequence of images acquired using the microscope is analyzed using image-processing techniques to detect motion in the image frames. There have been many successful experiments, including the study of protein-protein interactions [9], intercellular trafficking [10], and the motion of influenza molecules in planar bilayers [11].

Manuscript received January 6, 2006; revised May 16, 2007. This work was supported in part by ARO ODDR&E MURI01 under Grant DAAD19-01-0465 (Center for Communicating and Networked Control Systems, through Boston University).

The author is with the Department of Aerospace and Mechanical Engineering, Boston University, Boston, MA 02215 USA (e-mail: sanderss@bu.edu).

Color versions of one or more of the figures in this paper are available online at http://ieeexplore.ieee.org.

Digital Object Identifier 10.1109/TNB.2007.909014

As an example of the limitations of this approach, consider the assembly of RNA polymerase-DNA complexes. In [12], [13], sequential AFM images, separated by between 37 s to 2 min, were compared to determine the activity of RNA polymerase. However, RNA polymerase has been shown to translocate along natural double stranded DNA templates at a maximal speed of between 12 and 19 bases per second during transcription [14] and thus this approach is far from imaging the transcription of a single base. While recent results using optical trapping methods have achieved near base-pair resolution [15] the measurements are indirect. In order to achieve the goal of direct measurement of the transcription of a single base, new control techniques are needed.

Motivated by such considerations, researchers are striving to decrease the imaging time while maintaining image quality. Efforts have included tuning the components of the microscope [16], using cantilevers with very high natural frequency [17], controlling the quality factor of the probe [18]–[20], application of image tracking ideas to compensate for lateral drift [21], model-based control [22], [23] and stroboscopic techniques for periodic processes [24].

All of these approaches utilize the standard raster-scan pattern. This pattern can be viewed as an open-loop control scheme since no use is made of the data coming from the microscope. Often the sample of interest is string-like, including examples such as nanowires, carbon nanotubes, DNA, actin, microtubules, and the boundary of two-dimensional structures such as cells and crystals. For this type of sample, under the raster-scan approach most of the imaging time is wasted in obtaining completely uninteresting data about the substrate.

In this work we take a new approach to steering the tip. Similar to work on developing efficient sampling techniques for bit error rate diagrams [25], the central idea is to reduce the area to be sampled. For imaging string-like samples we utilize *local raster-scanning*. The algorithm is inspired by curvature-based control ideas for vehicle formations [26], [27] and models the sample as a planar curve. Data acquired by the tip is used in real-time to estimate the curve parameters. These estimates are filtered using a Kalman filter and are used to track the path defined by the sample with the tip. The approach and experimental results are presented in Section II.

In Section III we present a boundary tracking algorithm. The technique is related to work on contour tracking in image processing [28] and contour following using multiple sensor platforms [29], [30]. The algorithm begins with a closed curve surrounding the sample of interest. The tip of the AFM is scanned transverse to the curve and the data from the scan are used to update the closed curve such that it converges to the sample boundary. The algorithm is discussed and simulation results using real data obtained from AFM images of DNA tiles [31] are given.

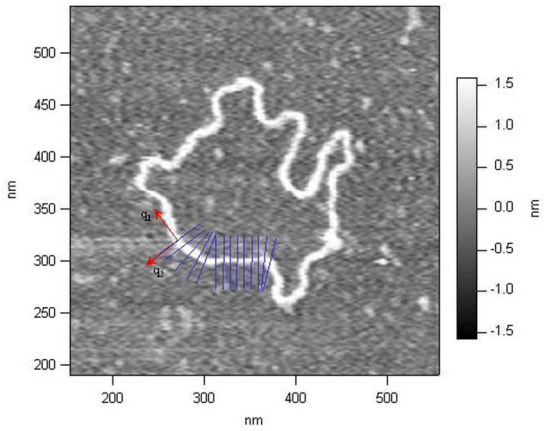

Fig. 1. AC-mode image of a DNA strand. Image courtesy of J. Park of the Rowland Institute at Harvard.

II. Local Raster-Scan

A string-like sample, such as the DNA strand in Fig. 1, can be modeled as a planar curve. To describe the spatial evolution of the curve, we utilize the Frenet-Serret frame. In the plane, this frame is defined at each point on the curve by the tangent vector and a (smooth) choice of normal vector to the curve. One such frame is shown in Fig. 1 with the tangent vector denoted as q_1 and the normal vector as q_2. The frame evolves in space according to

$$r'(s) = q_1(s) \tag{1a}$$
$$q_1'(s) = \kappa(s) q_2(s) \tag{1b}$$
$$q_2'(s) = -\kappa(s) q_1(s) \tag{1c}$$

where s is the arclength parameter, $\kappa(s)$ is the curvature at s, and prime denotes the derivative with respect to arclength. To image this sample we imitate the raster-scan pattern while ensuring that each scan line crosses the string perpendicular to the curve. Let v denote the scan speed and let a denote the width of the scan. Given a point on the curve $r(s)$ and the normal vector at that point, the desired path of the tip is given by

$$\dot{x}(t) = \pm v q_2(s), x(0) = r(s), t \in \left[\frac{-a}{2v}, \frac{a}{2v}\right] \tag{2}$$

where the overdot indicates derivative with respect to time. The tip is then advanced Δs units along the curve and another scan taken. A sequence of such scan lines is shown in Fig. 1.

The path $r(s)$ is not known *a priori*. However, given the frame and curvature at the current point, the next position can be estimated by appealing to the spatial evolution (1). We assume that the curvature changes slowly with respect to Δs and therefore take it as constant along one step. Recognizing that the sample is measured at discrete positions, we introduce the notation r_k for the kth sample along the string. Applying the variation of constants formula to solve (1) yields the update equations

$$r_{k+1} = r_k + \begin{cases} \frac{A_1(\kappa_k \Delta)}{\kappa_k} \begin{pmatrix} q_{1_k} \\ q_{2_k} \end{pmatrix}, & \kappa \neq 0 \\ q_{1_k} \Delta, & \kappa_k = 0 \end{cases} \tag{3a}$$

$$\begin{pmatrix} q_{1_{k+1}} \\ q_{2_{k+1}} \end{pmatrix} = A_2(\kappa_k \Delta) \begin{pmatrix} q_{1_k} \\ q_{2_k} \end{pmatrix} \tag{3b}$$

where

$$A_1(\cdot) = \begin{pmatrix} \sin(\cdot) & 0 & 1-\cos(\cdot) & 0 \\ 0 & \sin(\cdot) & 0 & 1-\cos(\cdot) \end{pmatrix},$$
$$A_2(\cdot) = \begin{pmatrix} \cos(\cdot) & 0 & \sin(\cdot) & 0 \\ 0 & \cos(\cdot) & 0 & \sin(\cdot) \\ -\sin(\cdot) & 0 & \cos(\cdot) & 0 \\ 0 & -\sin(\cdot) & 0 & \cos(\cdot) \end{pmatrix}.$$

A. Estimating the Position

Different types of data can be acquired by the microscope, depending on the imaging mode. Let N denote the number of measurements obtained in a single scan along a scan line. These measurements are modeled as

$$z_j = h_j + v_j, j = 1, 2, \ldots, N \tag{4}$$

where z_j is the measurement, h_j is the true value of the information at sample position j, and v_j are independent, identically distributed (iid) random variables. For simplicity, we assume that v_j is Gaussian with zero mean and variance σ_v^2, though other noise models can be accommodated. Rewriting (4) in vector form yields

$$Z = H + V, \quad V \sim \mathcal{N}\left(0, \sigma_v^2 \mathbb{I}\right). \tag{5}$$

The true data depends on the position of the sample in the scan. For example, when moving from the substrate onto the sample, the height signal undergoes a step up while the amplitude signal undergoes a brief change in magnitude until the low-level controller corrects for the change in height. In this paper we focus on using the height data and thus model the true signal as a step function. The extension to other signals is straightforward.

A variety of techniques may be used to estimate the position of the sample in a single line scan. Here we present a maximum likelihood approach. Let j^* denote the first data point in the scan which is of the sample rather than of the substrate. The shape of the sample can be approximated by the function

$$h_j = \begin{cases} 1, & j \geq j^*, \\ 0, & \text{else.} \end{cases} \tag{6}$$

Note that this is only a crude approximation to the true shape and that it assumes no knowledge of the actual height. However, it is sufficient to determine the point of transition from the substrate and is thus adequate for the estimation problem. This is related to a two-hypothesis problem wherein the detector must determine whether the tip is on the sample or not. See [32] for work along these lines.

The maximum likelihood (ML) estimator is given by

$$j^* = \arg \max_{m \in [1,N]} p(Z \,|\, m) \tag{7}$$

where $p(Z \,|\, m)$ is the conditional probability distribution function (pdf) for obtaining the measurement Z given that $j^* = m$. If the measurement noise v_j is modeled as a zero mean Gaussian process with variance σ_v^2 then the conditional pdf for the measurements is

$$p(Z \,|\, m) = \alpha e^{-\sum_{j=1}^{N} \frac{(z_k - \chi_m(j))^2}{2\sigma_v^2}} \tag{8}$$

where α is the normalizing factor and $\chi_{m^*}(\cdot)$ is the characteristic function defined by

$$\chi_m(j) = \begin{cases} 1, & j \geq m, \\ 0, & \text{else.} \end{cases} \tag{9}$$

Using this in (7) and taking the log likelihood, the ML estimator is

$$j^* = \arg \min_{m \in [1,N]} \sum_{k=1}^{N} (z_j - \chi_m(j))^2. \tag{10}$$

Due to the discontinuity of the characteristic function, a closed-form solution cannot be found from differentiation. A smooth model could be chosen in place of the step function to permit an analytical expression. However, in practice the number of samples along the short scan lines is small and thus an exhaustive search can be done rapidly. The estimate of the current position of the sample curve, $\hat{r}_k$, is then the position corresponding to sample point j^* in the current scan.

B. Estimating the Curvature and Heading Direction

The tangent and normal vectors are given by

$$q_{1_k} = \begin{pmatrix} \cos(\theta_k) \\ \sin(\theta_k) \end{pmatrix}, \quad q_{2_k} = \begin{pmatrix} -\sin(\theta_k) \\ \cos(\theta_k) \end{pmatrix} \tag{11}$$

where the heading angle, θ_k, is the angle q_{1_k} makes with the $x-$axis of the global reference frame. Given position estimates for two adjacent points on the string, the tangent vector can be estimated using a simple finite difference approximation, that is

$$\hat{q}_{1_k} = \frac{\hat{r}_k - \hat{r}_{k-n}}{||\hat{r}_k - \hat{r}_{k-n}||} \tag{12}$$

where $||\cdot||$ denotes the standard Euclidean metric. Here $n \geq 1$ is a fixed integer that can be chosen to offset difficulties arising from the small positional differences between points when the step size along the string is small. The estimate for the heading angle is then

$$\hat{\theta}_k = \text{atan2}([\hat{q}_{1_k}]_2, [\hat{q}_{1_k}]_1) \tag{13}$$

where $[q]_i$ denotes the ith component of q.

The curvature can be estimated using a geometric approach based on Heron's formula [33]. Let A, B, C be three successive and nearby points on a curve and let a, b, c denote the Euclidean distances between the points. The radius of curvature of the circle is then

$$\kappa(A, B, C) = \pm 4 \frac{\sqrt{l(l-a)(l-b)(l-c)}}{abc} \tag{14}$$

where $l = (1/2)(a+b+c)$ is the semiperimeter of the triangle. The estimate of the curvature of the string at the point r_k is given by (14) where the points A, B, C correspond to $\hat{r}_{k-2n}, \hat{r}_{k-n}$, and $\hat{r}_k$ respectively where again n is a fixed integer. (See [34] for more detailed comments on curvature estimation.) The sign is positive if the cosine of the angle between the vector connecting the points $\hat{r}_{k-n}$ and $\hat{r}_k$ and the normal vector is positive (so that the normal vector points "inside" the curve).

Because the heading and curvature estimators are numerical derivations of the position measurement, they amplify any noise in the estimate of $\hat{r}_k$. We therefore apply a Kalman filter by defining a linear system for the evolution of the curvature and heading angle. Under the assumption of constant curvature in a single step, the heading direction evolves according to $\theta_{k+1} = \theta_k + \kappa_k \Delta s$. The evolution of the curvature is modeled as a random walk. Defining the vector $X_k = (\theta_k, \kappa_k)$, this yields

$$X_{k+1} = FX_k + W_k, \tag{15a}$$

$$Y_k = HX_k + V_k \tag{15b}$$

where

$$F = \begin{pmatrix} 1 & \Delta \\ 0 & 1 \end{pmatrix}, \quad H = (\mathbb{1}). \tag{16}$$

We assume that the input and measurement noises have means

$$E[W_k] = \begin{pmatrix} 0 \\ \bar{w} \end{pmatrix}, \quad E[V_k] = \begin{pmatrix} 0 \\ 0 \end{pmatrix} \tag{17}$$

and covariances Σ and Γ respectively. The Kalman filter equations for this system are

$$\hat{X}_{k+1|k} = F\hat{X}_{k|k} + \begin{pmatrix} 0 \\ \bar{w} \end{pmatrix}, \tag{18a}$$

$$P_{k+1|k} = FP_{k|k}F^T + \Sigma, \tag{18b}$$

$$K_{k+1} = P_{k+1|k}H^T(HP_{k+1|k}H^T + \Gamma)^{-1}, \tag{18c}$$

$$\hat{X}_{k+1|k+1} = \hat{X}_{k+1|k} + K_{k+1}(Y_{k+1} - H\hat{X}_{k+1|k}), \tag{18d}$$

$$P_{k+1|k+1} = (\mathbb{1} - K_{k+1}H)P_{k+1|k} \tag{18e}$$

where the notation $\hat{X}_{k+1|k}$ indicates the estimate of X at time $k+1$ using data up to time k.

C. Discussion

To consider the reduction in imaging time possible using this algorithm, consider the DNA image in Fig. 1. The image is approximately 500 nm square and thus, to obtain a 2 nm lateral resolution, 250 scan lines are required using the traditional raster-scan pattern. If the tip moves at 1 μm/s (2 lines per second) the image will require 125 s to obtain. To obtain a similar resolution using the local raster-scan algorithm, assume that the step size is 2 nm. The total length of the DNA strand in the image is roughly 1 μm and so 500 steps are required to image the entire DNA. In solution, DNA is 2–3 nm in diameter [35]. To ensure each scan line fully crosses the strand, a scan line length of 10 nm is chosen. If the tip is moved at the same (average) speed as during the traditional raster-scan then each line will take 10 ms to complete and thus the entire DNA strand will be imaged in only 5 s.

The algorithm relies on the assumption that the change in the curvature of the sample between each scan line is small. If this assumption does not hold then the next predicted scan line may not cross the sample, resulting in a failure to track the path. Thus, in order to track highly varying curves, the step size must be small. However, a small step size is required to produce high resolution images and therefore this assumption is not overly restrictive. In addition, one can increase the length

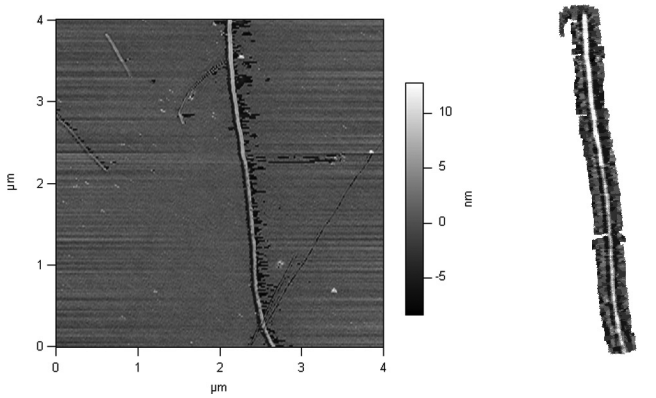

Fig. 2. Raster scan and local raster scan images of the same carbon nanotube. Note that most of the raster scan image is of the substrate while the local raster scan image is primarily of the nanotube. (Reprinted with permission from [36].

of the scan lines to ensure that the sample is crossed. However, as the length of the scan line increases it becomes more likely that other samples will be encountered and thus this approach must be handled with some care.

D. Experiments

Physical experiments were performed on carbon nanotube samples (provided by J. Park of the Rowland Institute at Harvard). Imaging was done using an AFM (Asylum Research MFP-3D) operated in ac mode. The local raster-scan algorithm was implemented in Igor Pro (WaveMetrics) and interfaced to the high-level control software of the microscope. While this allowed the algorithm to be implemented quickly, it introduced lengthy communication delays (on the order of 0.5–1 s) between each line scan. As a result the experiments achieved only modest reductions in scan times. However they do serve to illustrate the effectiveness of the technique.

In the left side of Fig. 2 we show an image of a carbon nanotube obtained using the traditional raster-scan pattern. The image is 4 μm square with 200 scan lines and 512 points along each line. The image resolution along the nanotube is therefore 20 nm. The tip velocity during the scan was 5 μm/s and the image took 401 s to acquire. The same portion of the nanotube was imaged using the local raster-scan algorithm. The algorithm was initialized near the lower end of the nanotube. The scan line length was set to 300 nm with a scan speed of 5 μm/s, as in the traditional raster-scan image. The average step size during imaging was 27.3 nm. The resulting image, shown in the right side of Fig. 2, was acquired in 197 s. Because the low-level controller was designed for the usual raster-scan pattern, it had difficulties when scanning short, arbitrarily oriented lines. As shown in Fig. 3, this resulted in uneven step sizes and limited the minimum step size with this implementation to approximately 10 nm. However, this difficulty is not innate to the actuators and can be overcome through proper controller design. In this example, the local raster-scan approach approximately halved the imaging time, despite the presence of long communication delays. Neglecting these delays, the image would have been completed in less than 20 s.

While the nanotube in Fig. 2 is fairly straight, the algorithm is not restricted to such straight paths. This is shown by the image

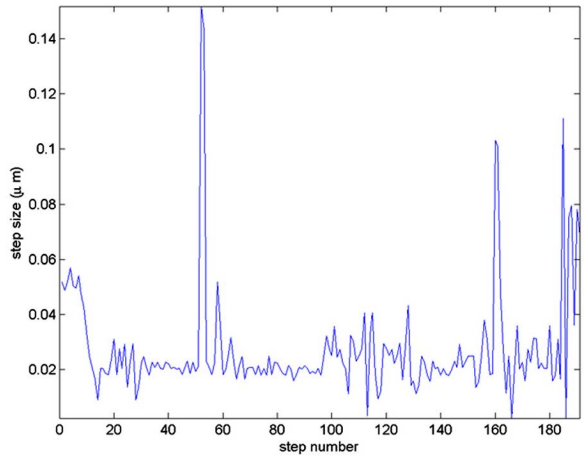

Fig. 3. Step sizes during the local raster-scan of the nanotube in Fig. 2.

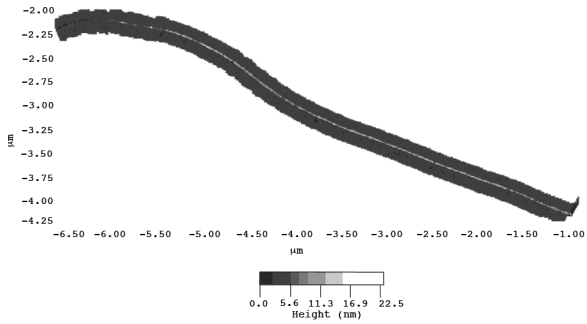

Fig. 4. Local raster-scan image of a long, curved carbon nanotube.

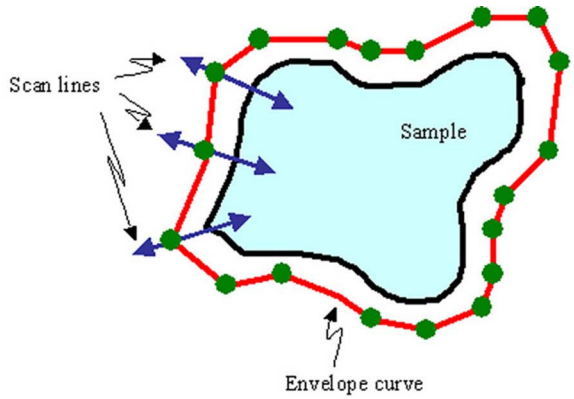

Fig. 5. An example of a sample and an envelope curve. The envelope curve is defined by a set of points. Associated to each point is a scan line. The AFM tip is moved along each scan line consecutively.

of a long, curved nanotube in Fig. 4. The average step size in this image was 17.4 nm.

III. Tracking Boundaries

The boundary to be tracked is assumed to form a continuous, closed curve. It is not assumed to be smooth nor concave. We surround the sample with a closed, piecewise linear curve referred to as the *envelope curve*. This curve is represented by a finite set of points, $p_j \in \mathbb{R}^2, j = 1, 2, \ldots, N$. Associated to each point is a scan line as shown in Fig. 5. (For clarity most of the scan lines have been left off the image.) The direction of each scan line is taken to be the bisector of the angle formed by the points p_{j-1}, p_j, p_{j+1} where we have adopted addition modulo

N for all subscripts. Let $\phi_j \in [-\pi, \pi], j = 1, \ldots, N$ denote these directions.

At the point p_j, the tip of the AFM is scanned along the direction ϕ_j towards the sample. The location of the edge of the sample in the scan can be estimated using the ML estimator described in Section II. Let $x_j \in \mathbb{R}$ denote the position of the sample in the scan taken at point p_j. This position varies over time due to the motion of the boundary. This (slow) movement is modeled as a collection of independent simple random walks, i.e.,

$$x_j(k+1) = x_j(k) + w_j(k) \tag{19}$$

where k indexes the number of times the scan has completed the envelope loop and $w_j(k)$ is a zero mean stochastic process. Under the assumption that the rate of change of the boundary of the sample is much slower than the update rate of the controller, the boundary may be viewed as fixed, that is, $w_j(k) = 0$.

The control in this scheme is the position of the points p_j. We seek to maintain the envelope curve at a constant distance away from the boundary. To achieve this, we want to drive the position of the boundary in the scan to a desired distance x_d along the scan line. Let q_j denote a unit vector pointing in the scan direction, i.e.,

$$q_j(k) = \begin{pmatrix} \cos(\phi_j(k)) \\ \sin(\phi_j(k)) \end{pmatrix}. \tag{20}$$

We define the update law

$$p_j(k+1) = p_j(k) - a(x_j(k) - x_d)q_j(k) \tag{21}$$

where $0 < a < 1$ is a gain. According to this law, the point p_j is moved along the scan direction either towards or away from the boundary depending on the error. Since x_j is the position of the sample in the scan line, a shift in p_j causes a corresponding shift in x_j. Using this in (19) yields

$$x_j(k+1) = x_j(k) - a(x_j(k) - x_d). \tag{22}$$

Define the error $e_j(k) = x_j(k) - x_d$. Then

$$\begin{aligned} e_j(k+1) &= x_j(k+1) - x_d \\ &= (1-a)e_j(k). \end{aligned} \tag{23}$$

Since $0 < a < 1$, this update law ensures that locally the envelope curve contracts to a distance x_d from the boundary. Under the assumption that the boundary moves slowly with respect to the update rate of the controller, the envelope curve will locally follow the boundary.

For practical implementation, the length of each scan line is fixed to a constant length L. If the sample is not encountered during the scan then x_k is defined to be ∞. The update law is modified to be

$$p_j(k+1) = \begin{cases} p_j(k) - a(x_j(k) - x_d)q_k, & x_j(k) \neq \infty, \\ p_j(k) - aL, & x_j(k) = \infty. \end{cases} \tag{24}$$

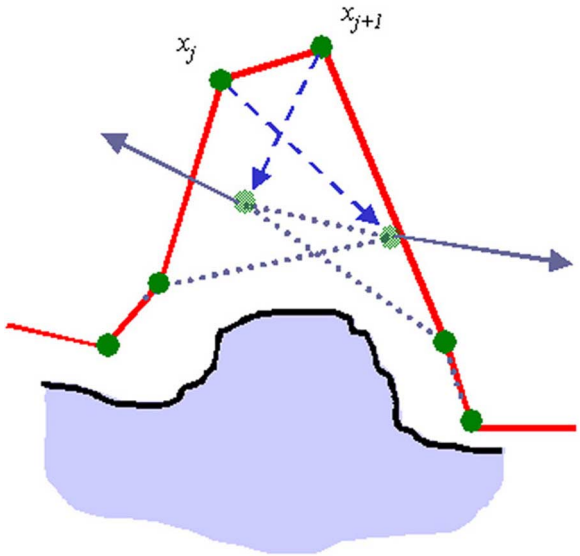

Fig. 6. If two points cross during an update step then a second loop is created. Because the next scan direction is directed away from the sample, the loop will grow without bound. This can be avoided by reordering the points after each update.

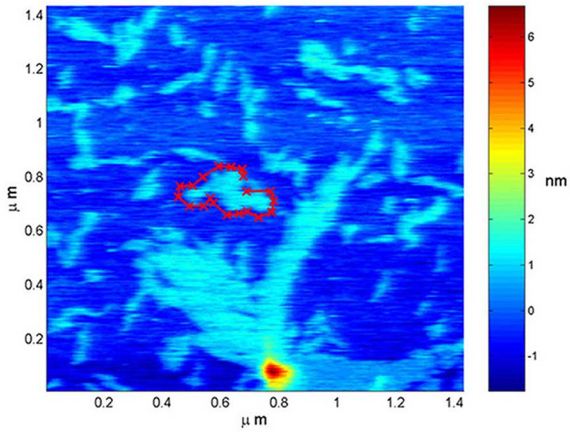

Fig. 7. Tapping-mode AFM image of DNA tiles.

to handle this. Note that in adopting this modified update law we have assumed the sample lies in the *positive* scan direction, that is along increasing x_j. This in turn implies that the envelope curve is simply connected and that the sample lies in the interior of the curve. Because the update law for p_j does not consider the positions of neighboring points, it is possible that during an update step, two adjacent points will cross, thereby creating a second enclosed region. At the next iteration, the positive scan direction will point *away* from the sample as shown in Fig. 6. As a result the loop will grow without bound once it is formed. This can be corrected by reordering the points after each update.

The spacing of the points p_j determines the image resolution along the boundary of the sample. As these points are updated, this spacing changes. Thus, after every update of the position the distance to the adjacent points must be checked. If the spacing between two adjacent points is too large, then a new point is added at the midpoint between the two. Similarly if the distance between two adjacent points is too small, then they are merged by defining a new point midway between them and deleting the

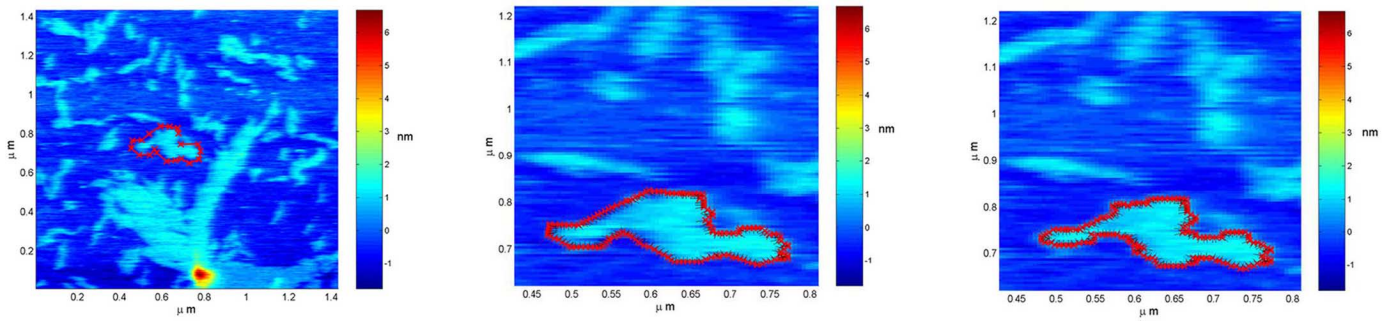

(a) (b) (c)

Fig. 8. Results of the first simulation. (a) Tapping mode AFM image of DNA tiles. The initial envelope curve for the simulation is indicated. This curve surrounds a crystal of DNA tiles. (b) The envelope curve after ten iterations of the algorithm (zoomed view). (c) The envelope curve after 20 iterations. The curve has converged to the boundary of the crystal.

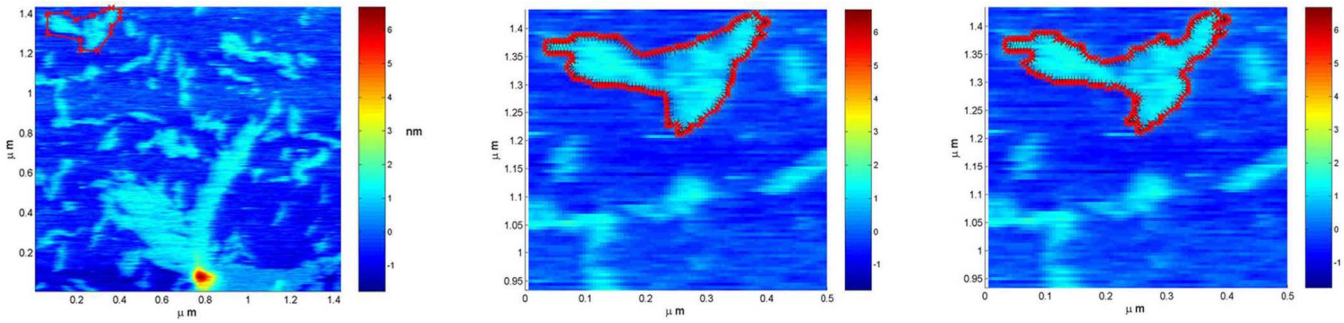

(a) (b) (c)

Fig. 9. Results of the second simulation. (a) The initial envelope curve was selected to surround a crystal in the upper right corner of the image. (b) The envelope curve after 20 iterations of the algorithm (zoomed view). (c) The envelope curve after 50 iterations.

two original points. Let Δs denote the desired spatial resolution. To prevent a chattering effect in adding and deleting points, a new point is added when the spacing is greater than $(3/2)\Delta s$ and points are merged when the spacing is less than $(1/2)\Delta s$.

To begin the algorithm, an initial envelope curve needs to be defined by the user. This can be achieved by first performing a low resolution, high-speed raster-scan with the microscope over the area of interest. The user can then select the set of points defining the initial curve based on the resulting image. A single iteration of the algorithm is defined to be one cycle around the envelope curve.

A. Discussion

Using the standard raster scan pattern, the time to image grows with the area; that is, it grows approximately as the *square* of a typical radius of the sample. The boundary, however, grows only *linearly* with this radius. Consider, for example, a simple triangular sample with a base of 900 nm and height of 900 nm. If this sample is imaged using the raster-scan pattern over a 1 μm square with 1 nm resolution at an average tip speed of 5 μm/s (5 Hz scan rate), then each frame will take 200 s to image. The perimeter of the triangle is $(1+\sqrt{2})900$ nm long. If the boundary-tracking algorithm is used with 1 nm steps along the perimeter and with each scan line being 30 nm with the average tip speed at 5 μm/s, then the perimeter will be imaged in only 21 s. Thus, the tracking algorithm promises a great reduction in the imaging time for the boundary of a sample.

It should be noted that a boundary is a string-like structure and therefore the local raster-scan algorithm described in Section II could be used to steer the tip along it. However, the approach in this section is guaranteed (for small enough gain) to converge to the boundary enclosed by the original envelope curve. It is possible, especially when the substrate is dense with samples (as in Fig. 7), that the local raster-scan algorithm would wander from boundary to boundary.

B. Simulations

Simulations were run using data from a sample of DNA tiles provided by Erik Winfree [31]. A sample of the tiles was deposited on freshly-cleaved mica and imaged using ac mode. The resulting image is shown in Fig. 7. The tip speed was set to 7 μm/s and the resolution in the plane was 5 nm. The data were imported into Matlab and the algorithm run in simulation on the data. Measurements were simulated by sampling 32 data points from the data set at equally spaced points along a given scan line.

For the first simulation, the control parameters were set to $\Delta s = 5.6$ nm, $L = 11$ nm, $x_d = 2.8$ nm, and $a = 0.5$ and the initial envelope curve shown in Fig. 8(a) was chosen. Notice that the enclosed DNA crystal has many sharp edges on its boundary. The envelope curve at 10 and 20 iterations is shown in Fig. 8(b)–(c). After 20 iterations the envelope curve has converged to the boundary of the crystal.

In Fig. 9(a) we show a second initial condition. For this simulation the gain was reduced to $a = 0.3$. The envelope curve at

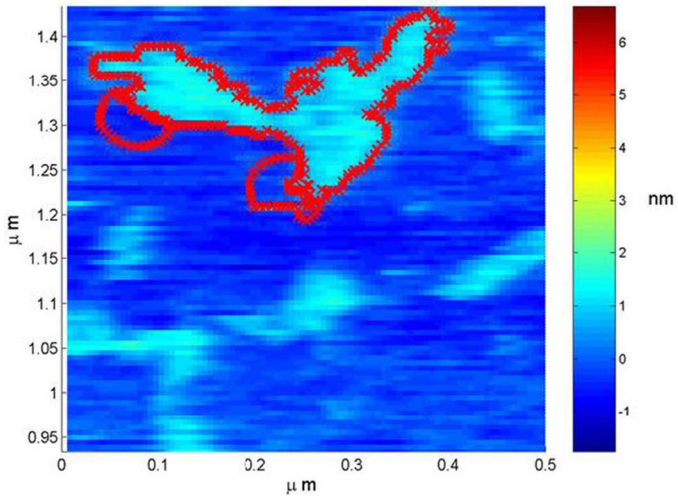

Fig. 10. A simulation with the gain set to $a = 0.7$. With this gain the algorithm points cross each other. As a result new loops are spawned and begin to grow. In this image two such loops have been created.

20 and 40 iterations is shown in Fig. 9(b)–(c). As before, the envelope curve converges to the boundary of the enclosed crystal.

Finally we show an example where the algorithm failed. The same initial condition as in Fig. 9(a) was chosen but in this case the gain was set to $a = 0.7$. The result after 14 iterations is shown in Fig. 10. Note that two new loops were spawned. According to the discussion above, these loops would grow without bound over subsequent iterations of the algorithm.

IV. Conclusion

In this paper we have presented two alternatives to the standard raster-scan pattern. Each algorithm takes advantage of data from the AFM in real time to keep the tip in the vicinity of the sample of interest. By reducing the area to be imaged, the time to acquire an image can be improved by an order-of-magnitude.

Acknowledgment

The author thanks Jiwoong Park of the Rowland Institute at Harvard for both the use of his AFM and for helpful discussions concerning the material in this paper, Roger Brockett of Harvard University for his insightful suggestions, and Erik Winfree of Caltech for the samples of self-assembling DNA tiles.

References

[1] H. G. Hansma, "Surface biology of DNA by atomic force microscopy," *Annu. Rev. Phys. Chem.*, vol. 52, pp. 71–92, 2001.
[2] Y. F. Dufrêne and G. U. Lee, "Advances in the characterization of supported lipid films with the atomic force microscope," *BBA-Biomembranes*, vol. 1509, no. 1–2, pp. 14–41, Dec. 2000.
[3] D. J. Müller, H. Janjovjak, T. Lehto, L. Kuerschner, and K. Anderson, "Observing structure, function and assembly of single proteins by AFM," *Prog. Biophys. Mol. Biol.*, vol. 79, no. 1–3, pp. 1–43, May–Jul. 2002.
[4] J. Ralston, I. Larson, M. W. Rutland, A. A. Feiler, and M. Kleijn, "Atomic force microscopy and direct surface force measurements (IUPAC technical report)," *Pure Appl. Chem.*, vol. 77, no. 12, pp. 2149–2170, 2005.
[5] J. Loos, "The art of SPM: Scanning probe microscopy in materials science," *Adv. Mater.*, vol. 17, no. 15, pp. 1821–1833, Aug. 2005.
[6] Y. L. Lyubchenko, "DNA structure and dynamics: An atomic force microscopy study," *Cell Biochem. Biophys.*, vol. 41, no. 1, pp. 75–98, Aug. 2004.
[7] N. C. Santos and M. A. R. B. Castanho, "An overview of the biophysical applications of atomic force microscopy," *Biophys. Chem.*, vol. 107, no. 2, pp. 133–149, Feb. 2004.
[8] M. Stolz, D. Stoffler, U. Aebi, and C. Goldsbury, "Monitoring biomolecular interactions by time-lapse atomic force microscopy," *J. Struct. Bio.*, vol. 131, no. 3, pp. 171–180, Sep. 2000.
[9] M. B. Viani, L. I. Pietrasanta, J. B. Thompson, A. Chand, I. C. Gebeshuber, J. H. Kindt, M. Richter, H. G. Hansma, and P. K. Hansma, "Probing protein-protein interactions in real time," *Nature Struct. Biol.*, vol. 7, no. 8, pp. 644–647, Aug. 2000.
[10] S. Kumar and J. H. Hoh, "Probing the machinery of intracellular trafficking with the atomic force microscope," *Traffic*, vol. 2, no. 11, pp. 746–756, Nov. 2001.
[11] T. Hughes, B. Strongin, F. P. Gao, V. Vijayvergiya, D. D. Busath, and R. C. Davis, "AFM visualization of mobile influenza a M2 molecules in planar bilayers," *Biophys. J.*, vol. 87, no. 1, pp. 311–322, Jul. 2004.
[12] M. Guthold, M. Bezanilla, D. A. Erie, B. Jenkins, H. G. Hansma, and C. Bustamante, "Following the assembly of RNA polymerase-DNA complexes in aqueous solutions with the scanning force microscopy," *Proc. Nat. Acad. Sci. USA*, vol. 91, no. 26, pp. 12927–12931, Dec. 1994.
[13] S. Kasas, N. H. Thomson, B. L. Smith, H. G. Hansma, X. Zhu, M. Guthold, C. Bustamante, E. T. Kool, M. Kashlev, and P. K. Hansma, "Escherichia coli RNA polymerase activity observed using atomic force microscopy," *Biochemistry*, vol. 36, no. 3, pp. 461–468, Jan. 1996.
[14] A. Kornberg, *DNA Replication*, 2nd ed. Herndon, VA: University Science Books, 2005.
[15] J. W. Shaevitz, E. A. Abbondanzieri, R. Landick, and S. M. Block, "Backtracking by single RNA polymerase molecules observed at near-base-pair resolution," *Nature*, vol. 426, no. 6967, pp. 684–687, Dec. 2003.
[16] T. Ando, N. Kodera, E. Takai, D. maruyama, K. Saito, and A. Toda, "A high-speed atomic force microscope for studying biological macromolecules," *Proc. Nat. Acad. Sci. USA*, vol. 98, no. 22, pp. 12468–12472, Dec. 2001.
[17] M. B. Viani, T. E. Schäffer, G. T. Paloczi, L. I. Pietrasanta, B. L. Smith, J. B. Thompson, M. Richter, M. Rief, H. E. Gaub, K. W. Plaxco, A. N. Cleland, H. G. Hansma, and P. K. Hansma, "Fast imaging and fast force spectroscopy of single biopolymers with a new atomic force microscope designed for small cantilevers," *Rev. Sci. Instrum.*, vol. 70, no. 11, pp. 4300–4303, Nov. 1999.
[18] J. Mertz, O. Marti, and J. Mlynek, "Regulation of a microcantilever response by force feedback," *Appl. Phys. Lett.*, vol. 62, no. 19, pp. 2344–2346, May 1993.
[19] T. Sulchek, R. Hsieh, J. D. Adams, G. G. Yaralioglu, S. C. Minne, C. F. Quate, J. P. Cleveland, A. Atalar, and D. M. Adderton, "High-speed tapping mode imaging with active Q control for atomic force microscopy," *Appl. Phys. Lett.*, vol. 76, no. 11, pp. 1473–1475, Mar. 2000.
[20] M. Antognozzi, M. D. Szczelkun, A. D. L. Humphris, and M. J. Miles, "Increasing shear force microscopy scanning rate using active quality-factor control," *Appl. Phys. Lett.*, vol. 82, no. 17, pp. 2761–2763, Apr. 2003.
[21] S. J. T. van Noort, K. O. van der Werf, B. G. de Grooth, and J. Greve, "High speed atomic force microscopy of biomolecules by image tracking," *Biophys. J.*, vol. 77, no. 4, pp. 2295–2303, Oct. 1999.
[22] G. Schitter, P. Menold, H. F. Knapp, F. Allgöwer, and A. Stemmer, "High performance feedback for fast scanning atomic force microscopes," *Rev. Sci. Instrum.*, vol. 72, no. 8, pp. 3320–3327, Aug. 2001.
[23] G. Schitter, R. W. Stark, and A. Stemmer, "Fast contact-mode atomic force microscopy on biological specimen by model-based control," *Ultramicroscopy*, vol. 100, no. 3–4, p. 2530257, Aug. 2003.
[24] M. Anwar and I. Rousso, "Atomic force microscopy with time resolution of microseconds," *Appl. Phys. Lett.*, vol. 86, no. 1, p. 014101, Jan. 2005.
[25] D. Y. Abramovitch, "Intelligent test point selection for bit error rate tester-based diagrams," U.S. Patent 6 745 148 B2, Jun. 2004.
[26] F. Zhang, E. Justh, and P. S. Krishnaprasad, "Boundary following using gyroscopic control," in *Proc. IEEE Conf. Decision and Control*, 2004, pp. 5204–5209.
[27] E. W. Justh and P. S. Krishnaprasad, "Equilibria and steering laws for planar formations," *Syst. Control Lett.*, vol. 52, no. 1, pp. 25–38, May 2004.
[28] M. Kass, A. Witkin, and D. Terzopoulos, "Snakes: Active contour models," *Int. J. Comput. Vis.*, vol. 1, no. 4, pp. 1573–1405, Jan. 1988.
[29] F. Zhang and N. E. Leonard, "Generating contour plots using multiple sensor platforms," in *Proc. IEEE Swarm Intelligence Symp.*, 2005, pp. 309–314.
[30] S. Susca, S. Martínez, and F. Bullo, "Monitoring environmental boundaries with a robotic sensor network," in *Proc. Amer. Control Conf.*, 2006, pp. 2072–2077.

[31] P. W. K. Rothemund, N. Papadakis, and E. Winfree, "Algorithmic self-assembly of DNA sierpinski triangles," *PLoS Biol.*, vol. 2, no. 12, pp. 2041–2053, Dec. 2004.
[32] D. R. Sahoo, A. Sebastian, and M. V. Salapaka, "Transient-signal based sample-detection in atomic force microscopy," *Physical Review Letters*, vol. 83, no. 26, pp. 5521–5523, Dec. 2003.
[33] E. Calabi, P. J. Olver, C. Shakiban, A. Tannenbaum, and S. Haker, "Differential and numerically invariant signature curves applied to object recognition," *Int. J. Comput. Vis.*, vol. 26, no. 2, pp. 107–135, Feb. 1998.
[34] F. Zhang, A. O'Connor, D. Luebke, and P. S. Krishnaprasad, "Experimental study of curvature-based control laws for obstacle avoidance," in *Proc. IEEE Int. Conf. Robotics and Automation*, 2004, pp. 3849–3854.
[35] M. Mandelkern, J. G. Elias, D. Eden, and D. M. Crothers, "The dimensions of DNA in solution," *J. Mol. Biol.*, vol. 152, no. 1, pp. 153–161, 1981.
[36] S. B. Andersson and J. Park, "Tip-steering for fast imaging in AFM," in *Proc. Amer. Control Conf.*, 2005, pp. 2469–2474.

Sean B. Andersson (M'00) received the B.S. degree in applied and engineering physics from Cornell University, Ithaca, NY, in 1994, the M.S. degree in mechanical engineering from Stanford University, Stanford, CA, in 1995, and the Ph.D. degree in electrical engineering from the University of Maryland, College Park, in 2003.

He is an Assistant Professor of Aerospace and Mechanical Engineering at Boston University, Boston, MA. His research interests include control applications in scanning probe microscopy, robotics, and symbolic control.